# Towards Surface-Enhanced Raman Scattering using electroless substrate for trace arsenic detection and speciation

Marie Adier, Anne-Marie Jurdyc, Bernard Dussardier, Charlotte Hurel, François Goutaland, Jean- Yves Michalon, Alexandre Merlen, Dominique Vouagner

*(work on progress)*

# Towards Surface-Enhanced Raman Scattering using electroless substrate for trace arsenic detection and speciation


## Authors

Marie Adier[1], Anne-Marie Jurdyc[1], Bernard Dussardier[2], Charlotte Hurel[2], François Goutaland[3], Jean-Yves Michalon[3], Alexandre Merlen[4], Dominique Vouagner[1]

## Affiliations

[1] Institut Lumière Matière (iLM), UMR5306 Université Lyon 1-CNRS, Université de Lyon 69622 Villeurbanne, France

[2] Université Côte d'Azur, CNRS, Institut de Physique de Nice (INPHYNI), UMR 7010, Nice, France

[3] Laboratoire Hubert Curien, UMR 5516 Université Jean Monnet, 42000 Saint Etienne, France

[4] Institut Matériaux Microélectronique Nanoscience de Provence (IM2NP), UMR 7334, Aix-Marseille Université, Université de Toulon, France



## Abstract

Arsenic is one of the most toxic elements present in the environment, especially in water. The World Health Organization (WHO) recommends a maximum concentration of arsenic in drinkable water of 10 µg/L (10 ppb). Sensors implementing Surface Enhanced Raman Scattering (SERS) can detect chemical species at low concentrations. The aim of this study is to compare two kinds of silver-coated SERS substrates for detection and speciation of trace, trivalent and pentavalent, inorganic arsenic compounds. One type of substrates were prepared by a classical thermal evaporation technique, the second type by an electroless process. The electroless substrates allow to differentiate As(3) and As(5) with a limit of detection (LOD) 1 µg/L (1 ppb) equal for each valency, below WHO recommendation. Though the SERS intensity shows a non linear behaviour over a large analyte concentration range of five orders of magnitude, these preliminary results are discussed the framework of the demonstration of a trace As SERS sensor in drinkable water.



## Keywords

Surface-enhanced Raman scattering ; Silver nanofilms ; Electroless deposition; thermal evaporation; arsenite detection ; arsenate detection; sensor


## Introduction

Arsenic (As) is the 20$^{th}$ most abundant element in the terrestrial crust. Global Arsenic pollution has become increasingly important because of its ecotoxicological consequences and especially its harmful effects on human health. Today, millions of people are exposed to elevated doses of As mainly for water, soil and food. That is why it is important to monitor water, food and soil with efficient, reliable and high-throughput As detection methods (Flora, 2015) (Singh & del Valle, 2015). In natural water, As is found as inorganic compounds : arsenite containing trivalent arsenic As(3) and arsenate containing pentavalent arsenic As(5). Arsenic is present in groundwater of 70 countries worldwide. The biggest scourge is the pollution of drinkable water causing poisoning of emerging-country populations. It can induce life-threatening diseases such as cancer in the long term. The World Health Organization (WHO)

recommendation sets the permissible concentration of As in drinkable water at 10 µg/L (10 ppb or 0.13 µM).

Inorganic As(3) and As(5) relative concentrations depend on the origin and the course of water. As(3) usually predomines in groundwater. When water surfaces or is extracted, contact to air provoques the partial oxidation into the other stable valency As(5). Also rain washing of the soil of polluted industrial sites induces seasonally varying total As concentration as well as the relative As(3) and As(5) concentrations (Chatterjee, Das, & Chakraborti, 1993). Industrial accidents may also cause massive river and soil pollution by heavy metals including Arsenic, like in the Animas River (Co., USA) in 2015 (Morgan, 2015) and in the Orbiel Valley (France) in 2018 (Dundas, Dekimpe, Lacharnay, Guggenheim, & Ide, 2019).

The reactivity and toxicity of As(3) is greater than that of As(5) (Fowler & Flora, 2015).Therefore the quantification of total As concentration is not sufficient to understand and quantify the degree of exposure of populations. Speciation is hence necessary to differentiate the absolute concentrations of As(3) and As(5), respectively, in order to provide reliable information for efficient environment survey. Finally, the monitoring of As total content and relative concentrations among As species is of interest to academic communities in geology and life science (Barats, Feraud, Potot, Philippini, & Travi, 2014).

The principal reference methods for speciation of trace As in natural water samples are Induced Coupled Plasma-Mass Spectrometry (ICP-MS) and Atomic Absorption Spectroscopy (AAS, and variants). These techniques are costly and time extensive. They need sample pre-treatment before analysis and are laboratory bound. ICP-MS requires a large amount of pure argon (Ma, Sengupta, Dongxing, & Dasgupta). Hence such techniques are impractical and difficult to implement, for field assays, especially in developing countries (Melamed, 2005). Some field test kits are commercially available. Reactive strips are based on the Gutzeit reaction (Ma, Sengupta, Dongxing, & Dasgupta). The reaction between As and strips containing arsine will cause it to stain. The colour of the strip is then compared with a colorimetric quantization scale. The disadvantages of this technique are that they are semi-quantitative tests, they form arsine (toxic) and they produce a large number of false positives and false negatives. Also, they do not allow for As(3) and As(5) speciation. Note that Raman spectroscopy would provide speciation, through vibrational fingerprint identification. However, the LOD of As by classical Raman scattering is as high as 23 g/L (Hao, et al., 2015). Electrochemical sensors are promising products; research and development is intense (Equipements Scientifiques SA; Metrhom, 2017; KLEARIA, s.d.). Their high sensitivity allows easy detection of As, down to 1µg/L. However, the presence of other metal ions in the water can cause interferences and distortion of the results, and the presence of an operator is necessary for the measurement.

Surface Enhanced Raman Scattering (SERS) is a promising technique for the field detection of As. Characterizing of molecules by SERS is commonly performed using noble metal nanoparticles like gold, silver (Ag) and copper. Under external electromagnetic field at an appropriate wavelength, metal nanostructures produce localized surface plasmon resonance (LSPR) defined as the collective oscillation of free electrons of metal (Degioanni, et al., 2015). The two well-known mechanisms to account for the origin of SERS are the electromagnetic (EM) and chemical or charge transfer (CT) mechanisms. Nanostructured Ag is a very sensitive material for SERS detection of As. The first detection of As by SERS was reported in 1988 by Greaves and Griffith, with a high concentration in As(V) (100 g/L). They used a suspension of Ag colloids as a SERS “volumic” substrate (Greaves & Griffith, 1988). The review of Hao et al. describes SERS properties of many chemically-processed Ag SERS substrates : mirror reaction, electroless process, Ag colloids, Ag nano wires by a two-phase interfacial self-assembly, etc (Hao, et al., 2015). The best Ag substrate in the scientific literature is an Ag nanoporous film doped with γ-$Fe_2O_3$ nanosheet and developed by Liu and al. (Liu, et al., 2015). Arsenic is adsorbed on a Ag-based hybrid nanocomposite surface. The LoD of this substrate is 1ppb for As(5) and 10 ppb for As(3), below WHO recommendation (Liu, et al., 2015). In the case of electroless substrate, Hao et al studied As(5) only, and detect it downto 5 µg/L, 5 times higher that WHO recommendation (Hao, Han, Xu, Li, & Meng, 2011). However, both of these manufacturing processes require several steps using basic compounds toxic to the environment.

Our aim is to study and demonstrate SERS substrates dedicated to heavy metal oxides, like As(3) and As(5) that are efficient, sensitive (below WHO recommendation), supporting a large concentration

range over several decades. They shall preferably be low-cost, versatile, easily attached to transductors like glass flat or cylindrical substrates (e.g. fiber cladding), as well as corrugated substrates (Degioanni, et al., 2015). Here we report on the study and comparison of two types of SERS substrates for As detection, elaborated by thermal evaporation and by electroless process, respectively. Both manufacturing processes are fast and require few steps. They need basic starting compounds with a low environmental toxicity, allowing appropriate use for detection measurements in natural as well as potable water. Physical deposition, such as thermal evaporation, is in principle more reproducible and repeatable than chemical deposition processes, but the former requires a more expensive facility, whereas the latter needs basic chemistry lab equipement.

After manufacture, we have characterized the deposited layers by AFM and optical extinction measurements (surface plasmon resonance). Then the SERS response of methylene blue (MB) solutions were characterized. MB is a well-known probe molecule used to evaluate the SERS effect (Vinod & Goppchandran, 2015). This molecule belongs to the dyes family characterized by a large value of polarizability leading to huge SERS signal (Tang, Zhu, Meng, & Wu, 2018). We conducted tests for detection and speciation of As(3) and As(5) over a wide range of concentrations. To the best of our knowldege, it is the first time that As-detection by SERS is performed on an Ag substrate made by a physical process. The results are discussed in the light of the experimental characteristics, such as plasmonic and structural properties including surface roughness. The variation of the SERS intensity relative to As(3) and As(5) signals as a function of analyte dilutions is also discussed as well as the adsorption of the arsenic mechanisms on the silver surface.

# Experimental

## -Silver SERS substrates elaboration

Two kinds of silver SERS layers were elaborated: electroless-deposited and thermally-evaporated layers. For both types of substrates, silver was deposited on glass slides. The slides were washed in a piranha solution (1/3 $H_2O_2$; 2/3 $H_2SO_4$) during 20 minutes and rinsed successively in an acetone bath for 5 minutes and an ethanol bath for 5 minutes. For the electroless process, the glass slides were immerged in a $SnCl_2$ solution (C=1g/L) during 15 minutes in order to sensitize the glass surface for silver deposition. Then, slides were put in the Tollen's reagent during 30 minutes by maintaining a vigorous agitation of the solution. The used Tollen's reagent was a silver nitride ($AgNO_3$) solution (C=0.03 mol/L) in ammonia medium with an adjusted pH at 8.8. The thickness of the electoless layer was 98 ± 5 nm , as measured by mechanical profilometry. For the thermal evaporation process, the layer deposition was performed in a home made vacuum chamber at a pressure of $6.10^{-6}$mbar. The initial current was 110 A, then lowered to 105 A. The silver layer thickness was controlled in situ using a quartz crystal scintillator. The initial growth speed was 2.0 nm/s, then 1.5 nm/s. The layer final thickness was 90 ± 5 nm.

## - Structural and optical characterization of the Ag SERS substrates

Roughness measurements were performed with a Bruker Dektak XT profilometer. The window scanning was 1mm for each measurement. Only the average roughness ($R_a$) was measured. AFM was performed in air, using a MFP-3D Asylum Research Oxford AFM. Images were recorded using a silicon cantilever. The grain size was determined with Gwyddion© software. The roughness was measured with the Dektak XT profilometer software.

Transmission extinction spectra were measured through the glass slides and the deposited layers with a UV-Visible-Near Infrared Perkin Elmer spectrophotometer. The measured light intensity transmitted though the samples were compared to a blanck glass slide as a reference. The spectral range extends from 300 to 1000 nm with 2-nm resolution.

### - Analytes elaboration for SERS measurements

Methylene blue (MB) solutions were prepared from MB powder and distilled water. The parent solution (1,00 ±0,02)*$10^{-1}$ mol/L was made with 3,2 g of MB powder in 100 mL of distilled water. The other solutions were prepared from successive dilutions of the parent solution, with a wide range of MB concentrations between 3,19.$10^{-6}$ g/L to 3,19 g/L. The pH of the solutions was between 6 and 6.5. The precision in the concentration of the diluted MB solutions is estimated to be 1 %.

The arsenic solutions were elaborated from standard arsenic solutions used for the calibration of mass spectrometry measurements. The As(3) standard solution had a concentration of 1000 ppm (1 g/L) and traces of NaOH. The As(5) standard solution had a concentration of 1000 ppm (1 g/L) and 2 % $HNO_3$. NaOH and $HNO_3$ do not interact with As detection by SERS (Xu, Hao, Li, & Meng, 2010). The concentration range of the diluted solutions was set between 0.1 g/L and 1 µg/L, below the WHO recommendation (10 µg/L). Table 1 lists the concentrations and pH of the As(3) and As(5) solutions. The precision in the concentration of the diluted As-solutions is estimated to be between 0.3 % and 1 %.

*TABLE 1 : Concentrations and pH of the diluted As(3) and As(5) solutions in water, respectively. The As(3) solutions contain traces of NaOH, whereas the As(5) solutions contain traces of $HNO_3$.*

| As(3) solutions | | As(5) solutions | |
|---|---|---|---|
| Concentration (g/L) | pH | Concentration (g/L) | pH |
| $10^{-1}$ | 11.9 | $10^{-1}$ | 1.4 |
| $10^{-2}$ | 10.9 | $10^{-2}$ | 2.1 |
| $10^{-3}$ | 9.1 | $10^{-3}$ | 3.0 |
| $10^{-4}$ | 6.1 | $10^{-4}$ | 3.5 |
| $10^{-5}$ | 6.5 | $10^{-5}$ | 4.0 |
| $10^{-6}$ | 5.7 | $10^{-6}$ | 4.5 |

### - Classical Raman and SERS measurements

Raman spectra were obtained with a fully confocal DXR ThermoFisher spectrophotometer operating at an excitation wavelength of 780 nm delivered by a frequency-stabilized single mode diode laser. A confocal 50-µm pinhole was set to allow measurements with a 2 µm depth resolution in an optically transparent sample. The laser power was set at 14 mW, corresponding to 9 mW incident power on the sample. The microscope magnification was x10 (Numerical Aperture = 0.25), leading to a laser spot diameter estimated at 4µm. The estimated power density on the sample was ~ 0.7 mW/µm$^2$. A high-resolution grating provided a spectral resolution of 3 cm$^{-1}$. The Rayleigh peak was cut by an edge filter included into the setup. Each measurement consisted of 20 exposures of 3 sec duration each. The background noise of the Raman and SERS measurements was less than 10 counts per second (cps). The limit of detection (LOD) was estimated from the crossing of the extrapolation of the SERS intensity vs concentration curves in semi-log scales with the abscissa axis.

SERS measurements of MB and arsenic (the analytes) were performed on samples at 780nm using the diluted solutions. They were carried out as follow: a droplet of analyte solution was deposited on the sample surface. The laser beam was focused at the interface between the sample surface and the drop. The repeatability conditions of the measurement were checked by performing the detection of analytes five times on the same substrates and the same drop of analytes, without changing any of the measurement parameters, in a short period of 20 minutes. This study was performed for all solutions of analytes and by the same experimenter. The reproducibility conditions of the measurement were checked by performing the measurement for the same dilutions of arsenic on three substrates of different series, with the same spectrophotometer and approximately the same volume of solution drop.

# Results and discussion

## Silver SERS substrates characterization

### Surface imaging of the silver SERS layers by AFM

The surface AFM images are shown on Figure 1 for both types of substrates. The average roughness ($R_a$) is estimated by mechanical profilometry. The arithmetic average of the absolute values of the deviations, between peaks and troughs is calculated. “Ra” measures the distance between this average and the “center line”. It clearly appears on Fig. 1(a) that the electroless-deposited silver layer is granular with inhomogeneous grain shapes and size. The grain or nanoparticle size is (101±10) nm and the average roughness ($R_a$) is (21±2) nm. On the opposite, the thermally-evaporated silver layer has a more continuous and less structured appearance, and is characterized by a low roughness value equal to (3±0,5) nm (Fig. 1(b).

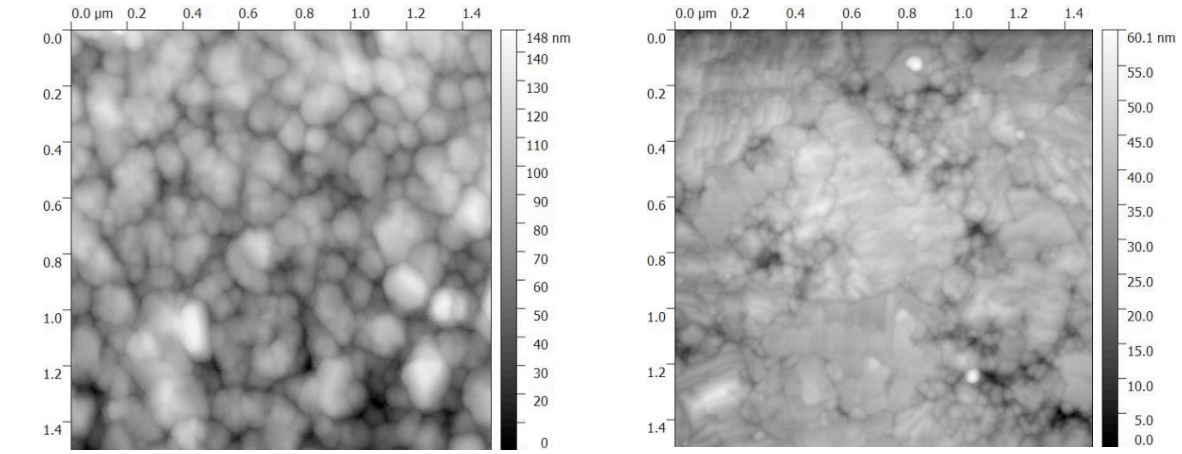


(a) (b)

*Figure 1 : AFM images : (a) Electroless-deposited silver layer ; (b) Thermally- evaporated layer. The total field of view is 1.5 µm x 1.5 µm. The thickness is coded on a grey scale, from blakc (0 nm) to white (148 nm (a) and 60.1 nm (b), respectively).*

### Plasmon band characterization of the silver SERS layers

Extinction spectra represented by the optical density versus wavelength are depicted Figure 2 for both kinds of SERS substrates. Both spectra show a general trend, that is an increasing optical density when wavelength increases. This is due to the wavelength sensitive reflectivity of silver films. However, one notice a large band with a maximum near 560 nm recorded for SERS substrates elaborated with an electroless-deposited silver layer (Fig. 2(a)). Usually the LSPR band maximum of spherical monodisperse silver nanoparticles is located near 420 nm (Mock, Barbic, Smith, Schultz, & Schultz, 2002). Nevertheless, a shift can be explained by different phenomena. The first hypothesis is due to the inhomogeneity of the geometry of nanoparticles deposit. This shift of the maximum is most likely due to the nanoparticles shape that is not spherical as shown by the AFM image of Figure 1a. Mock et al explain that there is a shift of the plasmon band position from 420 nm to 700nm, attributed to the shape and size of nanoparticles, that agrees with our results (Mock, Barbic, Smith, Schultz, & Schultz, 2002). Moreover, an inhomogeneous nanoparticle shape as observed in Figure 1(a) can also explain the silver plasmon band enlargement. Another hypothesis is that the silver films may have been partially oxidized into $Ag_2O$ between the elaboration and the absorption measurement. According to K. Chatterjee, a red shift in the plasmon band may be due to the presence of oxide on the silver surface (Chatterjee, Banerjee, & Chakravorty, 2002). They obtained an LSPR for oxide nanoparticles between 550 and 700 nm. Another cause may be a result from pollution by sulphur from ambient air. A thin layer of sulphur ($Ag_2S$) can shift the LSPR by around 100 nm (Mcmahon, Lopez, Meyer, Feldman, & Haglund, 2005). The last hypothesis is the presence of a strong coupling between Np_Ag (Halas, Lal, Chang, Link, & Nordlander, 2011; Quiroz, et al., 2019). This phenomenon can shift the LSPR by around 60 nm (Jain, Huang, & El-Sayed, 2005). This

hypothesis may explain the two observed bands around 380 nm, caused by quadrupole contributions, and around 560 nm, caused by dipole contributions (Kalfagiannis, Koutsogeorgis, Lidorikis, & Patsalas, 2017). Nevertheless, the observed red shift would contribute to the improvement of the plasmon excitation, and hence Raman exaltation and SERS, because the excitation wavelength (780 nm) is near the extinction band.

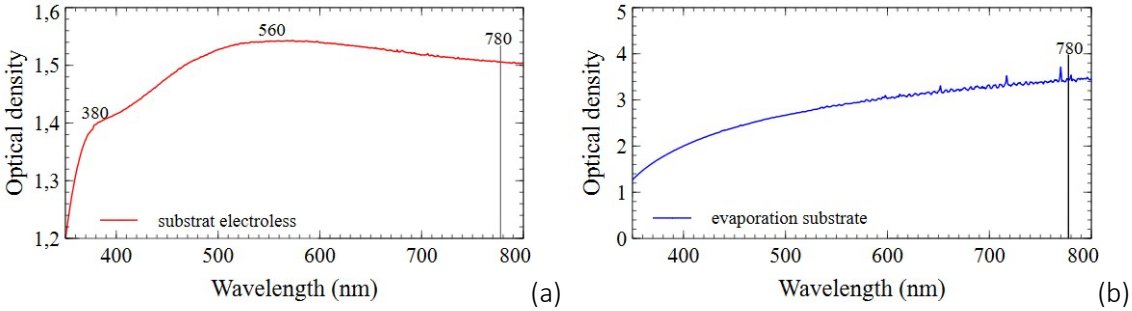


*Figure 2 : Optical density spectra of the SERS substrates with (a) Electroless-deposited silver layer, (b) Thermally-evaporated silver layer. 780 nm is the excitation wavelength*

Conversely, no resonance is observed on Figure 2(b) in the case of the substrate made by thermal evaporation. Instead of this, absorption increases uniformly throughout the visible range. This observation can be explained by several hypotheses. Since the measurements were carried out without an integrating sphere, the transmission spectrum obtained is in fact a reflectance spectrum (Jobst, et al., 2014). For thicknesses of the order of 90 nm deposited by evaporation, the percolation threshold is exceeded, and the film is semi-continuous (Figure 1 (b)). With this type of film, it is no longer possible to use optical absorption to measure the plasmonic response. According to Seal et al, in semi-continuous films obtained after the percolation threshold, there may be the coexistence of localized and delocalized plasmons. To demonstrate this coexistence, these authors used a near-field characterization technique, SNOM (Scanning Near-field Optical Microscopy) (Seal, et al., 2006).These techniques are difficult to implement because it is necessary to have ordered structural substrates to be able to interpret the results (A & F, 2014). On a thinner silver layer (about 5nm thick), we have observed a maximum attributed to LSPR around 420 nm (result not shown here). This value is in accordance with the literature for Np_Ag of circular shape (Mock, Barbic, Smith, Schultz, & Schultz, 2002; Smitha, Nissamudeen, Philip, & Gopchandran, 2008). However, this thin Ag coating peeled off when a droplet of As solution was deposited on it, due to surface tension and low adhesion power of Ag on glass. An adhesive undercoating would have overcome this, at the risk of generating parasitic Raman bands difficult to discriminate from the signal from arsenic. That is why the thermal-evaporated substrates with low silver thickness are not suitable for As detection by SERS.

### SERS efficiency evaluation of the substrates on methylene blue

We have estimated the LOD of MB and used it as a criterion to evaluate and compare the SERS efficiency of both types of substrates. Figures 3(a) and 3(b) show SERS spectra of a MB solution at $3{,}19.10^{-2}$ g/L recorded with both types of substrates. The most intense characteristic peaks of MB located at around 445 $cm^{-1}$ and 1625 $cm^{-1}$ are clearly visible. These bands are assigned to C-N-C skeletal bending vibrations and C-C stretching, respectively (Xiao & Shi-Qing, 2007) (Naujok, Duevel, & Corn, 1993). No MB band is detected for this diluted solution when MB is deposited directly on a bare glass substrate. This indicates that both types of substrates are SERS-efficient. Then, the SERS detection capacity of MB on both substrate types has been characterized using the prepared diluted MB solutions, over five orders of magnitudes in concentration. The spectra were all identical, except for the decreasing of signal strength and signal-to-noise ratio when the concentration decreases. In Figures 3(c) and 3(d), the intensities of the 1625 $cm^{-1}$ band are plotted against the MB concentration on both types of substrates, in log-log and semi-log scales, respectively. The LOD for the electroless substrate is ~$3.10^{-6}$ g/L whereas it is around $3.10^{-2}$ g/L for the thermally-evaporated one (Figure 3(d)), that is four orders of magnitude higher than for the electroless substrate. Note that the SERS signal from the electrolesss

substrates is much higher that from the thermally-evaporated one. It can be concluded that the electroless SERS substrate has a better SERS efficiency than the substrate made by evaporation.

In the literature, it is shown that the rougher the surface, the higher is the SERS performance. This higher SERS amplification is due to the increase of the surface area with roughness. On one hand, the electromagnetic wave is focused on the rough edges (Laor & Schartz, 1981; Pockrand, 1982; Rodriguez-Fernandez, et al., 2009). In addition, large scale roughness (10-200nm) promotes the molecule adsorption on the substrate promotes, and hence promotes the EM SERS mechanism [Brolo1997]. Moreover, when molecules are captured by, and adsorbed to plasmonic metal surfaces through chemical bonds, they can easily be excited by plasmons to generate SERS signals of their molecular fingerprints (Tang, Zhu, Meng, & Wu, 2018). In addition, the molecular adsorption is influenced by the concentration of solutions and can play a role on the Raman shift and on the intensities of the observed SERS peaks (Xiao & Shi-Qing, 2007; Chen, Jiang, Xu, & Lu, 1999; Naujok, Duevel, & Corn, 1993). However, no band shift was observed when the concentration changes during our measurements.

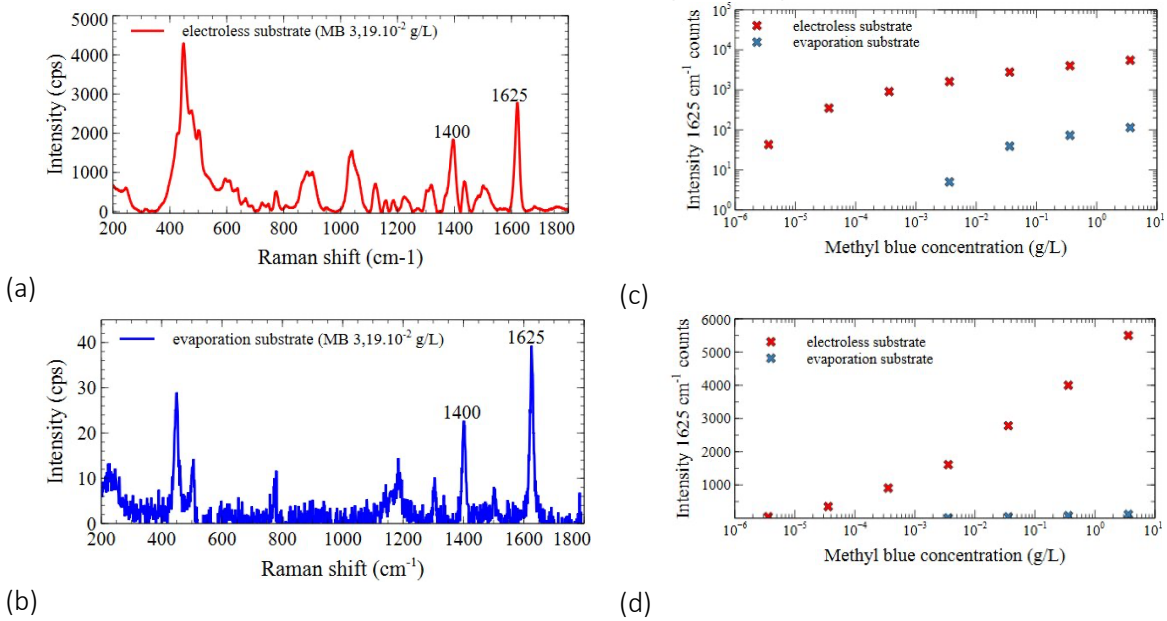


*Figure 3 : SERS spectra of MB (concentration3,19.10$^{-2}$ g/L) from (a) an electroless and (b)thermally-evaporated substrates (spectra without baseline). Peak intensity of the 1625-cm$^{-1}$ peak versus MB dilutions for both substrate types, in (c) log-log and (d) lin-log scales, respectively.*

The curves of SERS intensity vs concentrations (Figs 3(c) and 3(d)) show interesting features, particularly on the electroless substrate. This will be discussed below.

The intensity of the 1625 cm$^{-1}$ band increases uniformly with increasing concentration. Althougth the signal has a non linear behaviour *vs.* concentration (see below), no saturation is observed at high concentration (Fig. 3(d)). This indicates that the signal strength is directly linked to the adsorption of analytes on the substrate surface (Kneipp, Kneipp, Itzkan, R Dasari, & S Feld, 2002). In some cases, SERS bands intensity versus concentration laws can be established, such as linear, power or exponential laws, but usually on a very limited concentration range, typically less than order of magnitude (Sackmann & Materny, 2006). There are limitations of these laws towards higher concentrations since deviations due to saturation or geometrical effects cannot be avoided, and are highly dependent on experimental parameters.

Here we discuss on a phenomenologic law based on our observations over several orders of magnitude in analyte concentrations. The 1625-cm$^{-1}$ peak intensity versus MB concentration on the thermally-evaporated substrate (Fig. 3(d)) follows a logarithmic law of the form $I = a.\log_{10}(C) + b$, where $I$ is the signal intensity, $C$ the concentration, $a$ and $b$ are constants. However, the intensity curve of MB on the electroless substrate in Figure 3(d), is separated into two zones: each behaves “by parts” in a similar logarithmic manner, with an inflection near 3x10$^{-3}$ g/L where the $a$ and $b$ parameters change.

This behaviour change is likely due to the influence of the MB molecular adsorption geometry, with adsorption parallel (resp. perpendicular) to the silver surface at low (resp. high) concentrations (Zhong, Hu, & Xing, 2009). This change of behaviour was not observed from the thermally-evaporated substrates. Indeed, because of its lesser efficiency and sensitivity, the « inflection concentration » $3x10^{-3}$g/L was not reached, and the logarithmic law in the low concentration range was not observed.

## Arsenic detection by SERS

The As(3) and As(5) detection efficiency was evaluated for both types of SERS substrates in terms of LOD. This study has been done for a wide range of concentrations between $10^{-6}$ and $10^{-1}$ g/L for each species. Few literature studies have been conducted over such a wide concentration range for the study of As(5) and As(3).

### - As(3) detection

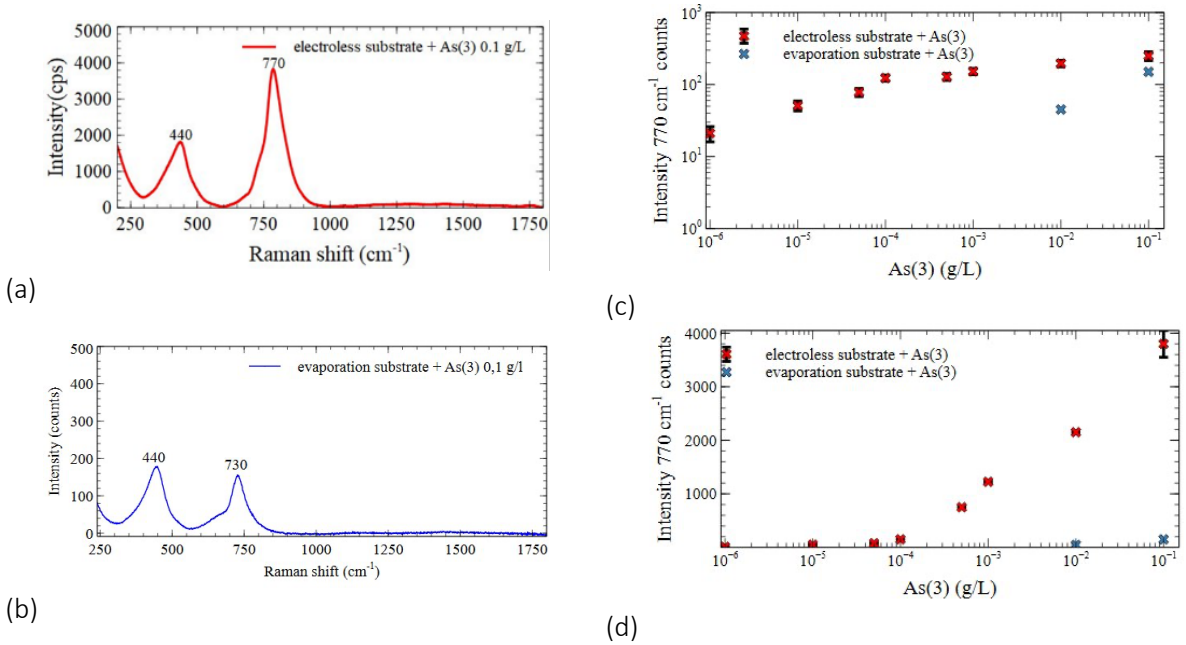


*Figure 4 : SERS spectra of a 0.1 g/L solution of As(3) from (a) an electroless substrate and (b) a thermally-evaporated substrate. SERS intensity of the peak around 730-770cm$^{-1}$ versus As(3) concentration for both substrate types in (c) log-log and (d) lin-log scales, respectively.*

The SERS spectra of an As(3) solution ($10^{-1}$ g/L) recorded on both types of substrates are shown in Figures 4(a) and 4(b). They show that both are SERS-sensitive for As(3) detection. The characteristic peaks of As (3) are visible: the peaks in the range 730-770 cm$^{-1}$ and 440 cm$^{-1}$ are assigned to the symmetric As-O and As-OH stretching vibrations, respectively. The most intense peak near 750 cm$^{-1}$ is used in the literature to plot As(3) SERS signal versus its concentrations (Hao, et al., 2015). Note that the Raman shift of this peak can vary from 720 to 770 cm$^{-1}$ (Goldberg & T., 2001), because it is sensitive to the nature of the substrate (functionalization, chemical terminal bond of the substrate surface), the excitation laser wavelength and the experimental conditions (Hao, et al., 2015).

The intensity of the peak from 730 or 770 cm$^{-1}$ is plotted versus As(3) dilutions on Figures 4(c) and 4(d) for both substrate types. The As(3) detection threshold (LOD) is $10^{-6}$ g/L using the electroless substrate, that is much lower than that measured with the thermally-evaporated substrate (~$5.10^{-3}$ g/L). Hence, As(3) can be detected below the WHO limit (10µg/L or $10^{-5}$g/L) using the electroless substrate. The change of slope in Figure 4(d) is discussed in the next section.

- As(5) detection

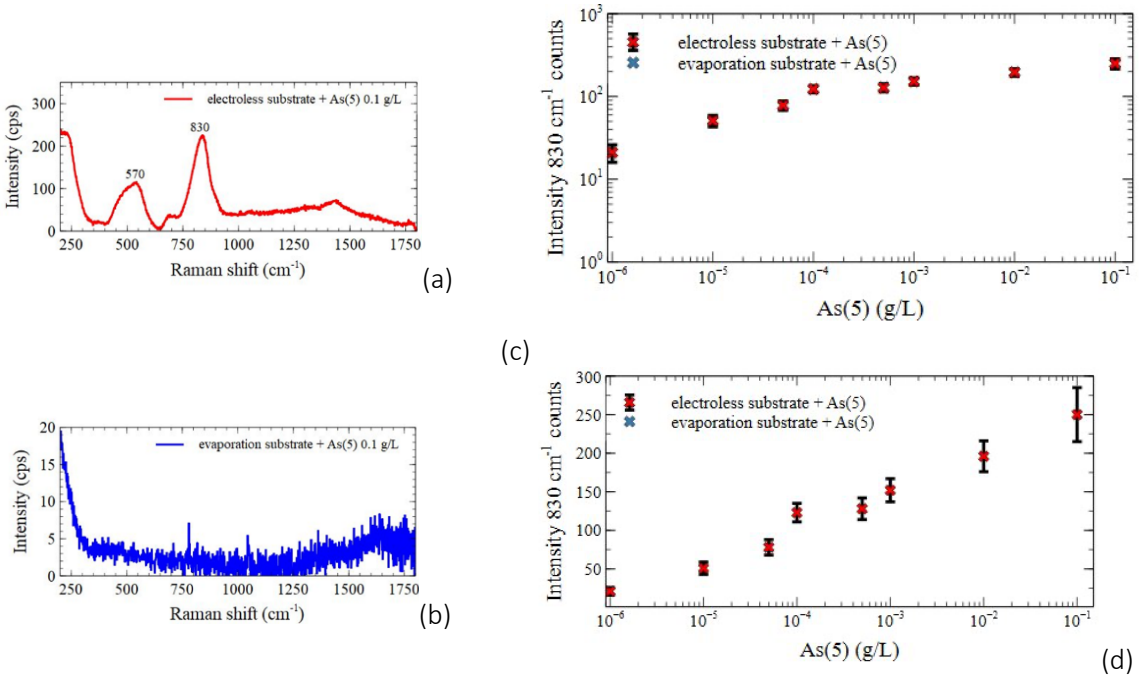


*Figure 5 : SERS spectra of a 0.1 g/L solution of As(5) with (a) an electroless substrate and (b) a thermally-evaporated substrate. SERS intensity of the 830-cm$^{-1}$ peak versus As(5) concentration in (c) log-log and (d) lin-log scales, respectively.*

Figures 5(a) and 5(b) present SERS spectra of an As(5) solution ($10^{-1}$ g/L) recorded for both kinds of SERS substrates, respectively. The characteristic peaks of As (5) are visible only in the case of the electroless substrate. The 830-cm$^{-1}$ peak at is assigned to the symmetric As-OH stretching vibration (Hao, et al., 2015; Goldberg & T., 2001; Mulvihill, Tao, Benjauthrit, Arnold, & Peidong, 2008) while the other peak at 570 cm$^{-1}$ is attributed to As-OH stretching vibration (Hao, et al., 2015). Figure 5(c) shows the plot of the 830-cm$^{-1}$ peak of As(5) intensity against As(5) concentration using both substrates types. The signal increase uniformly. The As(5) LOD is $10^{-6}$ g/L, much below the WHO recommendation ($10^{-5}$g/L). In our experimental configuration, the signal with the thermally-evaporated substrate produced only a noisy background (Fig. 5(b) and no plot of the signal vs concentration was possible.

It is interesting to compare the signal levels between As(3) and As(5) on the electroless substrate (Figures 4 and 5). Though the experimental conditions were identical for both Arsenic valancies, the signal observed for As(3) is around one order of magnitude higher that that from As(5). This would illustrate the better adsorbtivity of As(3) than As(5) onto the substrate. This is attributed to the more ionic nature of As(3). Another hypothesis to explain this difference is the possible presence of oxide or sulphur on the surface of the substrate. Indeed, As(3) has a better affinity with sulphur deposited on silver surface (Teixeira & Ciminelli, 2005). This would explain the fact that As(3) for high concentrations have a stronger SERS signal than As(5).This would agree with one of the hypotheses that explain the red shift of the plasmon resonance. The experimental testing of these hypotheses are under study.

## SERS intensity variation versus analyte dilutions with electroless silver substrates

The intensity of the 770-cm$^{-1}$ peak versus the concentration of As(3) on the electroless substrate on Figure 4(d) has a logarithmic behaviour in two parts,

$I = a.\log_{10}(C) + b$, where $I$ is the signal intensity, $C$ the concentration, $a$ and $b$ are constants (Figure 3(d)). Here the change of $a$ and $b$ parameters occurs around the concentration $10^{-3}$ g/L. A tentative interpretation relies on the observation that As(3) has two forms, depending on the pH of the solution. The pH of the solutions used here depend on the As(3) concentration (Table 1). Figure 6(a) and 6(c) show the concentration of As(3) and As(5) solutions as a function of pH and the associated Pourbaix diagram (Han, et al., 2013). At pH < 9, As(3) is in the non-ionic form $H_3AsO_3$, corresponding to concentrations less than $10^{-3}$ g/L. At pH > 9, As(3) is in the ionic form $H_2AsO_3^-$ for concentrations equal

and higher than $10^{-3}$ g/L. Because the silver surface is rather hydrophilic (Tang, Zhu, Meng, & Wu, 2018), it would tend to form metal/oxygen bonding in aqueous phase (Valette, 1982). From this, we conclude that the change of slope on the semi-log diagram Fig 4(c) is probably due to a change of adsorption rate that is caused by the change of ionic form of As(3).

In the case of As (5), the 830-$cm^{-1}$ peak intensity versus As(5) concentration follows a semi-logarithmic law of the same form (Figure 5(d))-(Xu, Hao, Li, & Meng, 2010)-(Han, Hao, & Xu, 2011). Unlike As(3), As(5) is always in the ionic form: $H_2AsO_4^-$ when pH<7 and $HAsO_4^{2-}$ when pH>7 (Figure 6b). This ionic stability would explain that no slope change is observed.

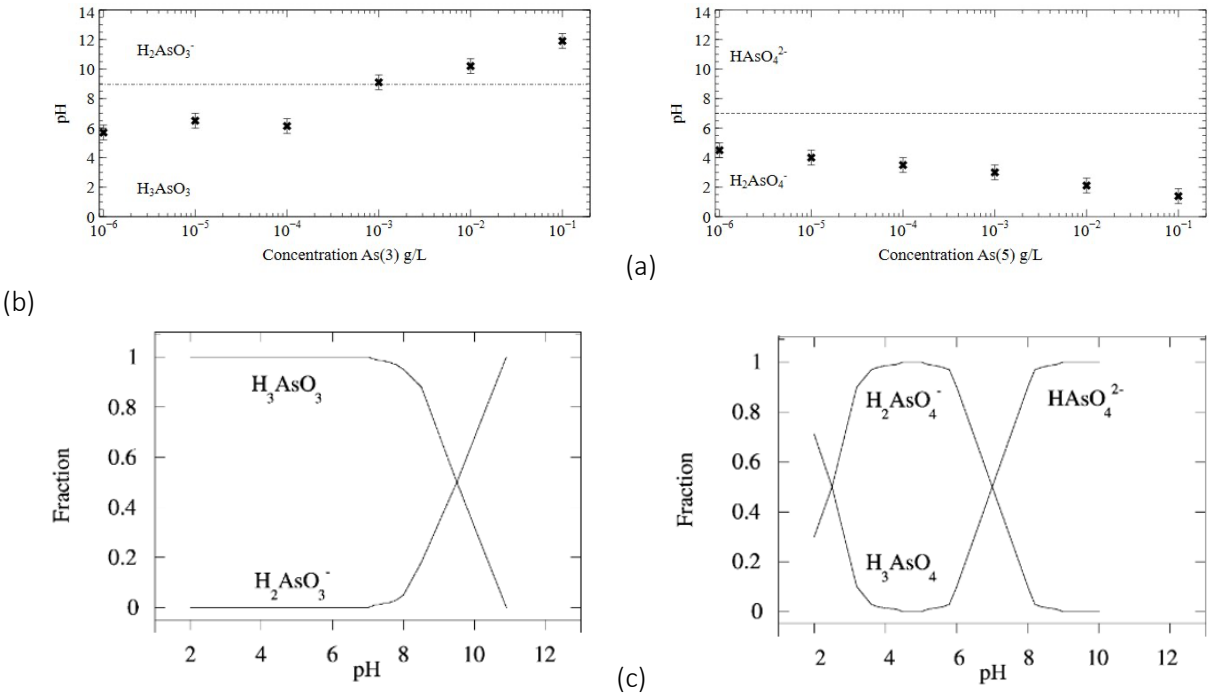


*Figure 6 : pH versus concentration for (a) As(3) and (b) As(5). Data are extracted from As Pourbaix Diagram for As(3) (c) and (d) As(5) (Han, et al., 2013)*

## Conclusion

In this study, we have compared the LOD of arsenite and arsenate, and the sensitivity for both species over a very large range of concentrations ($10^{-6}$-$10^{-1}$ g/L) on two types of SERS substrates. The substrates were made by an electroless and by a thermal evaporation method, respectively. The electroless substrate has a granular nanostructure and a high roughness (21 nm) while the other has a more continuous layer structure and a lower roughness (3 nm): this difference has a great influence on the SERS efficiency and on the measured LOD. On the thermally-evaporated substrates, the As(3) LOD was ~ $5.10^{-3}$ g/L (5 ppm) and no As(5) was detected. On the other hand, the electroless substrates are more efficient, with LOD =$10^{-6}$ g/L (1 ppb) for both As(3) and As(5). This is an order of magnitude less than the WHO recommendation of total As content in drinkable water. To our knowledge, the lowest As(3) LOD for silver nanofilm was $10^{-5}$ g/L (10 ppb). We have also shown a semi-logarithmic relationship between the SERS signal and the concentration. This relationship on such a wide range of concentrations would potentially serve as a calibration over 5 orders of magnitude in arsenic concentration, to help developping a sensor for trace As as well as for food industry (medium concentrations) and soils (accepteable threshold ~$7.10^{-3}$ g/kg (7 ppm) (Jha, et al., 2021), as well as production of medecine or materials containing arsenic (concentrations > $10^{-3}$ g/L).

The adsorption efficiency of As(3) is an order of magnitude higher than that of As(5) on the electroless substrates. This ratio could be explained by the presence of parasistic compounds on the silver surface (oxides or sulphurs) of the electroless substrate. These surface species may also explain

the redshift of the plasmon band. These hypotheses necessitate further investigations. Finally, although the electroless substrates were elaborated using basic and rather environmentally friendly chemicals, and laboratory equipements, it allowed a better detection of As than the physically deposited substrates. This would give a better potential to electroless technique for the demonstration and development of field sensors for the detection of Arsenic.

## Acknowledgements


- European Regional Development Fund (FEDER)-CNRS Université Côte d'Azur (OPTIMAL platform at INPHYNI)
- Université Côte d'Azur ,«Space, Environment, Risk and Resilience» Academy of Excellence
- GIS GRIFON, Groupement d'Interêt Scientifique « GRoupement d'Initiatives pour les Fibres Optiques Nouvelles », CNRS, France
- Wolfgang Doeblin Federation of Research (UCA Nice, CNRS)-France


## AUTHOR DECLARATIONS

The authors have no conflicts to disclose.

## DATA AVAILABILITY

The data that support the findings of this study are available within the article.

## References


A, M., & F, L.-L. (2014). Imaging the Optical Near Field in Plasmonic Nanostructures. *Applied Spectroscopy, 68*(12), 1307-1326.

Barats, A., Feraud, G., Potot, C., Philippini, V., & Travi, Y. (2014, March 01). Alpine/Mediterranean Var River watershed (France). *Science of the Total Environment, 473-474*, 422-436. doi:https://doi.org/10.1016/j.scitotenv.2013.12.007

Chatterjee, A., Das, D., & Chakraborti, D. (1993, January 01). A study of ground water contamination by arsenic in the residential area of Behala, Clacutta due to industrial pollution. *Environmental Pollution, 80*(1), 57-65. doi:https://doi.org/10.1016/0269-7491(93)90010-L

Chatterjee, K., Banerjee, S., & Chakravorty, D. (2002). Plasmon resonance shifts in oxide-coated silver nanoparticles. *Physical Review B, 66*(8), 085421_1-085421_7.

Chen, W.-X., Jiang, H., Xu, Z.-D., & Lu, Y. (1999). Study on the chemisorption kinetics of Methylene Blue using SERS technique. *Chinese Journal of Chemistry, 17*(2), 125-131.

Degioanni, S., Jurdyc, A. M., Cheap, A., Champagnon, B., Bessueille, F., Coulm, J., . . . Vouagner, D. (2015). Surface-enhanced Raman scattering of amorphous silica gel adsorbed on gold substrates for optical fiber sensors. *ournal of Applied Physics, 118*(15), 153103.

Dundas, M., Dekimpe, V., Lacharnay, J., Guggenheim, J., & Ide, M.-C. (2019, Febuary 15). *Arsenic pollution: A toxic legacy of France's gold rush.* Consulté le October 20, 2021, sur https://www.france24.com/en/20190216-down-earth-france-pollution-gold-mine-arsenic-toxic-waste-salsigne-aude

Equipements Scientifiques SA. (s.d.). *Metalyser HM1000.* Consulté le Aout 20, 2019, sur https://www.es-france.com/index.php?controller=attachment&id_attachment=6512

Flora, S. J. (2015). Arsenic: Chemistry, Occurrence, and Exposure. Dans *Handbook of Arsenic Toxicology* (pp. 1-49). Elsevier Inc.

Fowler, B. A., & Flora, S. (2015). Arsenical Kidney Toxicity. Dans A. Press (Éd.), *Handbook of Arsenic Toxicology* (pp. 349-361). Oxford: Elsevier. doi:https://doi.org/10.1016/B978-0-12-418688-0.00014-9

Goldberg, S., & T., J. C. (2001). Mechanisms of Arsenic Adsorption on Amorphous Oxides Evaluated Unsing Macroscopic Measurements, Vibrationnal Spectroscopy, and Surface Complexation Modeling. *Journal of Colloid and Interface Science, 234*, 204-216.

Greaves, S. J., & Griffith, W. P. (1988). Surface-enhanced Raman scattering (SERS) from silver colloids of vanadate, phosphate and arsenate. *Journal of Raman Spectroscopy, 19*(8), 503-507.

Halas, N. J., Lal, S., Chang, W.-S., Link, S., & Nordlander, P. (2011). Plasmons in Strongly Coupled Metallic Nanostructures. *Chemical Reviews, 111*(6), 3913-3961.

Han, C., Li, H., Pu, H., Yu, H., Deng, L., Huang, S., & Luo, Y. (2013). Synthesis and characterization of mesoporous alumina and their performances for removing arsenic(V). *Chemical Engineering Journal, 217*, 1-9.

Han, M.-J., Hao, J., & Xu, Z. M. (2011). Surface-enhanced Raman scattering for arsenate detection on multilayer silver nanofilms. *Analytica Chimica Acta, 692*(1-2), 96-102.

Hao, J., Han, M.-J., Han, S., Meng, X., Su, T.-L., & Wang, Q. K. (2015). SERS detection of arsenic in water : a review. *Journal of environnemental sciences, 36*, 152-162.

Hao, J., Han, M.-J., Xu, Z., Li, J., & Meng, X. (2011). Fabrication and evolution of multilayer silver nanofilms for surface-enhanced Raman scattering sensing of arsenate. *Nanoscale Research Letters, 6*(1), 263.

Jain, P. K., Huang, W., & El-Sayed, M. A. (2005). On the Universal Scaling Behavior of the Distance Decay of Plasmon Coupling in Metal Nanoparticle Pairs: A Plasmon Ruler Equation. *Nano Letters, 7*(7), 2080-2088.

Jha, G., Mukhopadhyay, S., Ulery, A. L., Lombard, K., Chakraborty, S., Weindorf, D. C., . . . Brungard, C. (2021, May 01). Agricultural soils of the Animas River watershed after the Gold King Mine spill: An elemental spatiotemporal analysis via portable X-ray fluorescence spectroscopy. *Journal of Environmental Quality, 50*(3), 730-743. doi:https://doi.org/10.1002/jeq2.20209

Jobst, P. J., Stenzel, O., Schürmann, M., Modsching, N., Yulin, S., Wilbrandt, S., . . . Tünnermann, A. (2014). Optical properties of unprotected and protected sputtered silver films: Surface morphology vs. UV/VIS reflectance. *Advanced Optical Technologies, 3*(1), 91-102. doi:https://doi.org/10.1515/aot-2013-0052

Kalfagiannis, N., Koutsogeorgis, D. C., Lidorikis, E., & Patsalas, P. (2017). Laser Annealing as a Platform for Plasmonic Nanostructuring. Dans *Nanoplasmonics - Fundamentals and Applications.* InTech.

KLEARIA. (s.d.). *The lab-on-a-chip that revolutionises water analyses PANDa*. Récupéré sur https://www.klearia.com/panda-analyzer

Kneipp, K., Kneipp, H., Itzkan, I., R Dasari, R., & S Feld, M. (2002). Surface -enhanced Raman scattering and biophysics. *Journal of physics condensed mattter*(14), R597-R624.

Kolozsi, A., Lakatos, A., Galbács, G., Madsen, A. Ø., Larsen, E., & Gyurcsik, B. (2008). A pH-Metric, UV, NMR, and X-ray Crystallographic Study on Arsenous Acid Reacting with Dithioerythritol. *Inorganic Chemistry, 47*(9), 3832-3840.

Laor, U., & Schartz, C. (1981). The role of surface roughness in surface enhanced raman spectroscopy (SERS) the importance of multiple plasmon resonances. *Chemical physics letters, 83*(2), 566-570.

Liu, R., Sun, J.-f., Cao, D., Zhang, L.-q., Liu, J.-f., & Jiang, G.-b. (2015). Fabrication of highly-specific SERS substrates by co-precipitation of functional nanomaterials during the self-sedimentation of silver nanowires into a nanoporous film. *Chemical Communications, 51*(7), 1309-1312.

Ma, J., engupta, M. K., uan, D., & Dasgupta, P. K. (2014). Speciation and detection of arsenic in aqueous samples: A review of recent progress in non-atomic spectrometric methods. *Analytica Chimica Acta, 831*, 1-23. doi:10.1016

Ma, J., Sengupta, M. K., Dongxing, Y., & Dasgupta, P. K. (s.d.). Speciation and detection of arsenic in aqueous sample : A review of recent process in non-atomic spectrometric methods.

Mcmahon, M. D., Lopez, R., Meyer, H. M., Feldman, L. C., & Haglund, R. F. (2005). Rapid tarnishing of silver nanoparticles in ambient laboratory air. *Applied Physics B, 80*(7), 915-921.

Melamed, D. (2005). Monitoring arsenic in the environment: a review of science and technologies with the potential for field measurements. *Analytica Chimica Acta, 532*(1), 1-13.

Metrhom. (2017, juin 22). *946 Portable VA Analyzer (scTRACE Gold)*. Consulté le Aout 20, 2019, sur https://www.metrohm.com/fr-fr/products-overview/voltammetry/946-portable-va-analyzer/29460010

Mock, J. J., Barbic, M., Smith, D. R., Schultz, D. A., & Schultz, S. (2002). Shape effects in plasmon resonance of individual colloidal silver nanoparticles. *The Journal of Chemical Physics, 116*(15), 6755-6759.

Morgan, E. (2015, August 10). Durango copes with 'orange nastiness' of toxic sludge river pollution. *The guardian*. Consulté le October 20, 2021, sur https://www.theguardian.com/us-news/2015/aug/10/colorado-spill-animas-river-durango-toxic-orange

Mulvihill, M., Tao, A., Benjauthrit, K., Arnold, J., & Peidong, Y. (2008). Surface-Enhanced Raman Spectroscopy for Trace Arsenic Detection in Contaminated Water. *Angewandte Chemie International Edition, 47*(34), 1433-7851.

Naujok, R. R., Duevel, R. V., & Corn, R. M. (1993). Fluorescence and Fourier Transform surface-enhanced Raman scattering measurements of methylene blue adsorbed onto a sulfur-modified gold electrode. *Langmuir, 9*(7), 1771-1774.

Perderson, L. (1982). Comparison of stannous and stannic chloride as sensitizing agents in the electroless deposition of silver on glass using X-ray photoelectron spectroscopy. *Solar Energy Materials, 6*(2), 221-232.

Pockrand, I. (1982). Surface-enhanced raman scattering from evaporated Ag films : size of revelant roughness features and range of classical enhancelent. *Chemical physics letter, 93*(5), 509-513.

Quiroz, A., Sato, R., Massoni, E., Sánchez, R., Bañuelos, G., Sánchez, N., & Mata, E. (2019, October 23). Step by step synthesis of silver films by electroless technique and their SERS application of sodium arsenate. (I. Publishing, Éd.) *Materials Research Express, 6*(11), 116439. doi:10.1088/2053-1591/ab4c74

Rodriguez-Fernandez, J., M. Funston, A., Perez-Juste, J., A. Alvarez-Puebla, R., M. Liz-Marzan, L., & Mulvaney, P. (2009). The effect of surface roughness on the plasmonic response of individual sub-micron gold sphere. *Physical Chemistry Chemical Physics, 11*, 5909-5914.

Sackmann, M., & Materny, A. (2006). Surface enhanced Raman scattering (SERS) a quantitative analytical tool? *Journal of Raman Spectroscopy, 37*(1-3), 305-310.

Seal, K., Genov, D. A., Sarychev, A. K., Noh, H., Shalaev, V. M., Ying, Z. C., . . . Cao, H. (2006, Novembre 17). Coexistence of Localized and Delocalized Surface Plasmon Modes in Percolating Metal Films. (A. P. Society, Éd.) *Physical Review Letters, 97*(20), 206103. doi:10.1103/PhysRevLett.97.206103

Singh, M., & del Valle, M. (2015). Arsenic Biosensors: Challenges and Opportunities for High-Throughput Detection. In *Handbook of Arsenic Toxicology* (pp. 575-588). Elsevier Inc.

Smitha, S., Nissamudeen, K., Philip, D., & Gopchandran, K. (2008, Novembre 1). Studies on surface plasmon resonance and photoluminescence of silver nanoparticles. *Spectrochimica Acta Part A: Molecular and Biomolecular Spectroscopy, 71*(1), 186-190. doi:https://doi.org/10.1016/j.saa.2007.12.002

Tang, H., Zhu, C., Meng, G., & Wu, N. (2018). Review—Surface-Enhanced Raman Scattering Sensors for Food. *Journal of The Electrochemical Society, 165*(8), B3098-B3118.

Teixeira, M. C., & Ciminelli, V. S. (2005). Development of a Biosorbent for Arsenite: Structural Modeling Based on X-ray Spectroscopy. *Environmental Science & Technology, 39*(3), 895-900.

Valette, G. (1982). Hydrophilicity of metal surfaces silver, gold and copper electrodes. *Journal of Electroanalytical Chemistry and Interfacial Electrochemistry, 139*(2), 285-301.

Vinod, M., & Goppchandran, K. (2015). Bi-metallic Au-Ag nanochains as SERS substrates. *Current Applied Physics, 15*, 857-863.

Xiao, G.-N., & Shi-Qing, M. (2007). Surface-enhanced Raman scattering of methylene blue absorbed on cap-shaped silver nanoparticles. *Chemical Physics Letters, 447*, 305-309.

Xu, Z., Hao, J., Li, F., & Meng, X. (2010). Surface-enhanced Raman spectroscopy of arsenate and arsenite using Ag nanofilm prepared by modified mirror reaction. *Journal of Colloid and Interface Science, 347*, 90-95.

Xu, Z., Jing, C., Hao, J., Christodoulatos, C., Korfiatis, G. P., Li, F., & Meng, X. (2012). Effect of Bonding Interactions between Arsenate and Silver Nanofilm on Surface-Enhanced Raman Scattering . *The Journal of Physical Chemistry C, 116*(1), 325-329.

Zhong, L., Hu, Y., & Xing, D. (2009). Adsorption Orientation of Methylene blue (MB+) on the Silver Colloid: SERS and DFT Studies. *Conference on Lasers and Electro-Optics/Pacific Rim 2009*.